# The Etched Hourglass Nebula MyCn18: I. *Hubble Space Telescope* Observations

Raghvendra Sahai[1], Aditya Dayal[1,2], Alan M. Watson[3], John T. Trauger[1], Karl R. Stapelfeldt[1], Christopher J. Burrows[4], John S. Gallagher III[5], Paul A. Scowen[6], J. Jeff Hester[6], Robin W. Evans[1], Gilda E. Ballester[7], John T. Clarke[7], David Crisp[1], Richard E. Griffiths[8], John G. Hoessel[5], Jon A. Holtzman[9], John Krist[4], Jeremy R. Mould[10]

Received ______________________; accepted ______________________

---

[1]Jet Propulsion Laboratory, MS 183-900, California Institute of Technology, Pasadena, CA 91109

[2]IPAC/ JPL, MS 100-22, California Institute of Technology, Pasadena, CA 91125

[3]Instituto de Astronomía, Universidad Nacional Autónoma de México, J. J. Tablada 1006, 58090 Morelia, Michoacán, México

[4]Space Telescope Science Institute, 3700 San Martin Drive, Baltimore, MD 21218

[5]Department of Astronomy, University of Wisconsin, Madison, 475 N. Charter Street, Madison, WI 53706

[6]Department of Physics and Astronomy, Arizona State University, Tyler Mall, Tempe, AZ 85287

[7]Department of Atmospheric, Oceanic, and Space Sciences, University of Michigan, 2455 Hayward, Ann Arbor, MI 48109

[8]Department of Physics, Carnegie Mellon University, Pittsburgh, PA 15213-3890

[9]Dept. of Astronomy, New Mexico State University, Box 30001 Dept. 4500, Las Cruces, NM 88003-8001

[10]Mount Stromlo and Sidings Springs Observatories, Australian National University, Weston Creek Post Office, ACT 2611, Australia

## ABSTRACT

We have obtained emission-line and continuum images of the young planetary nebula MyCn18 with the Wide-Field Planetary Camera 2 on the Hubble Space Telescope. Although from the ground MyCn18 appeared to have a triple-ring structure similar to SN 1987A, the HST images show that MyCn18 has an overall hourglass shape. A series of arcs appear to be etched on the walls of the hourglass near its rims. In the complex central region of the nebula we find a small, inner hourglass structure and two rings. Ring 1 is a bright elliptical ring and Ring 2 a smaller higher-excitation ring. The outer and inner hourglass and Ring 1 all have different centers, and none are coincident with the central star.

The hourglass shape of the main nebula is consistent with the predictions of the generalised interacting winds hypothesis for planetary nebula formation. However, the complex inner nebular structure of MyCn18 and the offset of the central star from the center of the nebula remain a mystery. We discuss several mechanisms for producing the offset of the central star. Although none are found to be completely satisfactory, those involving a binary central star probably offer the best hope of successful explanation.

*Subject headings:* planetary nebulae: individual (MyCn18), stars: AGB and post–AGB, stars: mass–loss, circumstellar matter

## 1. Introduction

MyCn18 (PK307-4°1) is a planetary nebula (PN) named after its discoverers, Mayall & Cannon (1940). Schwarz, Corradi, & Melnick (1992) obtained ground-based images which show a striking resemblance to the triple-ring nebula around SN1987A (Burrows et al. 1995). Corradi & Schwarz (1993) (hereafter CS93) obtained images and long-slit spectra of MyCn18 and concluded from optical and near-infrared diagnostics that it is a young PN. The Of(h) central star has an effective temperature of 51,000 K. The nebular expansion velocity determined from [O III]$\lambda$5007 emission is 10 km s$^{-1}$(Gleizes, Acker & Stenholm 1989), lower than the value indicated by the 48 km s$^{-1}$ velocity spread seen in the [N II]$\lambda$6548 spectrum (CS93). As is true for most PNs, the distance to MyCn18 is uncertain and estimates span a broad range from 800 to 3200 pc. More recent determinations favor larger distances and in this paper we have followed CS93 and adopted 2.4 kpc.

We have obtained images of MyCn18 with the Wide Field & Planetary Camera 2 (WFPC2) on the *Hubble Space Telescope.* We present these images here and use them to investigate the structure of MyCn18. In §2 we describe our observations. In §3 we present our observational results. In §4 we discuss how the nebula might have formed. In §5 we summarise our results and conclusions. Detailed spatio-kinematic modelling of the nebula, which will be of particular use to theorists attempting to match gas-dynamic models to this nebula, is presented in a following paper (Dayal et al 1999, hereafter Paper 2).

## 2. Observations

MyCn18 was imaged using the Planetary Camera of WFPC2, which has a field of view of $34'' \times 34''$ and scale of $0\farcs0456$/pixel (Trauger et al. 1994). Observations were made in 4 narrow-band filters dominated by [O I], [N II], H$\alpha$, and [O III] emission lines and one line-free medium-band filter (F547M). Table 1 is a summary of the observations. Standard procedures were used to reduce and calibrate the images. Cosmic rays were removed by comparing two equal exposure images, when available, or by scanning through the images with a $5 \times 5$ pixel window, determining all pixels with intensity $3\sigma$ above the median value, and replacing them with nearest-neighbour interpolated values.

## 3. Results

Figure 1 shows images of the whole nebula and Figure 2 shows images of the central region in each of our filters. The H$\alpha$ and [N II] emissions are similarly distributed and clearly show an hourglass-shaped nebula. The measured fluxes of the nebula are given in Table 1. The H$\alpha$ flux has been corrected for contamination by [N II] $\lambda$6548 emission using our measured [N II] $\lambda$6586 flux and the filter transmission curves. Acker et al. 1989 give H$\alpha$ & [O III] fluxes of $8.3 \times 10^{-11}$ & $2 \times 10^{-11}$ erg s$^{-1}$ cm$^{-2}$, but these values are based on extrapolating the flux measured through a $4'' \times 4''$ aperture to the full size of the nebula (details about the extrapolation are not available) and are likely to be inaccurate.

Visual inspection of the H$\alpha$ and [N II] images suggests that the top (south-eastern) half of the hourglass is tilted towards us, an orientation consistent with published spectroscopic data (CS93)[11].

The F547M image is dominated by nebular *continuum emission* rather then weak *line emission* or scattered light from the star. The only significant nebular line in the filter is [N II] 5755 Å, whose strength relative to H$\alpha$ suggests that it contributes less than 3% of the observed emission (Acker et al. 1989). The theoretical ratio of nebular continuum to H$\alpha$

[11]the sign of the declination increments in their long-slit spectrum is flipped – H. Schwarz 1995, private communication

flux suggests that the former has a flux density of about 9.5 Jy (Osterbrock 1989; Brown & Mathews 1970). The closeness of this to the 9.8 Jy we measure suggests that light scattered by dust makes an insignificant contribution. This conclusion is further bolstered by the similarity between the radial profiles in H$\alpha$ and continuum emission (Fig. 3).

### 3.1. The Components and Structure of the Nebula

We now describe the different structural components of MyCn18, together with the relative distribution of H$\alpha$, [N II], and [O III] emission (Fig. 4). Figure 4a is a false-color image showing the [N II] (red), H$\alpha$ (green), and [O III] (blue) emission; each image has been processed in order to emphasize sharp structures. The color balance has been adjusted such that regions where the [N II] and H$\alpha$ overlap appear orange. In figures 4b and 4c, we show the [N II]/H$\alpha$ and [O III]/H$\alpha$ ratio images. The false-color and ratio images show that (as expected) the [O III] emission, a tracer of higher excitation gas, is more centrally confined than [N II] emission, a tracer of lower excitation gas – the [O III]/[N II] intensity ratio in the outer orange regions is smaller by factors of ~30-100 compared to the greenish-blue central region. The line-ratio images will be useful for constraining detailed photo-ionisation models of the MyCn18 nebula: such modelling is outside the scope of this paper.

The nebular structure can be divided into several distinct regions as a function of observed distance from the geometrical center of the nebula. Outside the bright hourglass walls, there is weak emission with both smooth and filamentary components. This emission is visible only in the [N II] and H$\alpha$ images. At both ends of the hourglass we find a bright rim, followed by a region of mottled emission. The mottled structure is seen prominently in the more distant part of the SE rim and the nearer part of the NW rim. The elongated knots in the mottled region are roughly 2–5 pixels (220–550 AU) wide and 5–10 pixels (550–1100 AU) long. It difficult to determine if any mottled structure is present in the other sides of the hourglass because of foreshortening. Moving inwards, we find a region characterised by a system of arcs. These resemble etchings on the walls of an hourglass. The etchings have FWHM of roughly 4-6 pixels (440-660 AU). Both the mottled structure and the etchings show a larger contrast relative to neighbouring nebulosity in [N II] than in H$\alpha$ (see Fig. 4b) – the values of the [N II] contrast ratio lie in the range 1.7-2.5 and are typically 10-35% higher than those for H$\alpha$. The mottling and etchings disappear at smaller radii, and the walls of the hourglass present a smoother appearance. The [N II]-to-H$\alpha$ ratio is higher in the etched/mottled regions compared to the smooth region by a factor 1.5 (see Fig. 3). The nebula measures about 18" along its long axis, and has a maximum width of about $8''\!.5$.

In the innermost region, we find a pair of intersecting elliptical rings which appear to be the rims of a small inner hourglass (see Figure 2a). Within this hourglass, we find Ring 1, a bright, roughly elliptical (size $1''\!.8\times1''\!.4$) ring (Figure 2b), which delineates the waist of the hourglass structures. Within Ring 1 is Ring 2, a smaller *incomplete* ring of size $0''\!.8\times1''\!.2$ (Figure 2d). Ring 2 is seen prominently in H$\alpha$ & [O III], but is almost invisible in [N II] & [O I]. This indicates that it consists of more highly-excited gas than Ring 1, presumably because it is closer to the central star. There is a local minimum of emission in the central region of Ring 1.

Moving to much larger scales, Figure 5 shows a false-color image from all four cameras of WFPC2 of the region around the bright nebula. Of particular interest are the blobs of distant, faint nebulosity located along the long axis of the nebula. The blobs are fainter in [O III] than in H$\alpha$ or [N II] and appear to lie at a projected distance of $33''$ or $1.3\times10^{18}$ cm from the center of MyCn18. They probably belong to the larger collection of blobs representing a knotty, bipolar 500 km s$^{-1}$ outflow from MyCn18 (Bryce et al. 1997). A rough estimate of the mass of ionised gas within each of these blobs derived from their

H$\alpha$ flux, assuming T$_e$=(0.5-2)$\times 10^4$ K, is a few$\times 10^{-5} M_\odot$. The mass of these blobs can be compared to the total nebular mass of MyCn18, estimated by modeling its IRAS far-infrared fluxes using the 2-component dust emission model of Sahai et al. (1991) (and scaling by a typical gas-to-dust ratio). The color-corrected IRAS fluxes used are 2.0, 22.5, 22.4 and 12.6 Jy at 12, 25, 60, and 100 $\mu$m. Assuming a dust emissivity of 150 cm$^2$g$^{-1}$ at 60 $\mu$m (Jura 1986), with a $\lambda^{-p}$ power-law variation and $p$=1.0(1.5), we find that the masses and temperatures of the 2 components are 3.3(5.6)$\times 10^{-4}$ and 0.4(1.1)$\times 10^{-6}$ $M_\odot$ and 89(75) and 160(132) K. We convert this to a total nebular mass of $\sim$(0.02–0.1) $M_\odot$, using the poorly known gas-to-dust ratio in PNs, which spans a range of values from 50 in the Ring Nebula (Zhang et al. 1994) to 200 typical of the circumstellar envelopes (CSEs) of Asymptotic Giant Branch (AGB) stars. The size of the thermally emitting dust region is roughly comparable to the optical nebula seen in the HST images: given a bolometric luminosity $L_{\rm bol}$ of 990 $L_\odot$ (§3.3) and $T_{\rm eff} = 51,000$ K, we find that dust grains reach the temperature derived above at a distance of $\sim 5 \times 10^{17}$ cm from the central star (e.g. Herman, Burger & Penninx 1986, Zhang et al. 1994). We conclude that the mass of gas ejected in the high-velocity blobs is a factor $10^{-3}$ or less of the total nebular mass of MyCn18.

### 3.2. Centers and Misalignments

The strong symmetry of the nebular structures in MyCn18 allows us to locate their centers accurately and show that the outer and inner hourglasses, Ring 1 and Ring 2 have different centers and none are centered on the central star. The major axis of the nebula has a position angle of $152° \pm 0.5°$. The central star does not lie on the major axis but is offset along the minor axis (roughly westwards) from the geometrical centers of the outer hourglass, the inner hourglass, Ring 1, and Ring 2 by 2.5$\pm$0.5 pixels (270 AU), 10.5$\pm$1 pixels (1150 AU), 6$\pm$0.5 pixels (650 AU), and 4$\pm$0.5 pixels (440 AU), respectively. The greater relative brightnesses of the western sides of Ring 1 and Ring 2 in H$\alpha$ and [O III] appear to be consistent with the central star's offset to the west.

### 3.3. The Central Star

Photometry of the central star in F547M image gives $m_V$=14.90±0.05. This implies a blue magnitude $m_B$=14.47±0.05 (ignoring interstellar extinction) for $T_{\rm eff} = 51,000$ K, in agreement with the ground-based value of $m_B$=14.4±0.5 (Tylenda et al. 1991). The bolometric flux estimated by integrating the observed flux distribution (CS93) over all wavelengths (from 0.36–100 $\mu$m) is $5.5\times10^{-9}$ erg s$^{-1}$ cm$^{-2}$, giving a luminosity $L_{\rm bol} \approx 990 L_\odot$ for a distance of 2.4 kpc. The above derivation is likely to underestimate $L_{\rm bol}$ because large parts of the nebula are density bounded (Paper 2), allowing a significant fraction of the stellar radiation at wavelengths less than 912Å to escape undetected from the nebula. The central star is probably surrounded by hot dust in the waist region because the expected K-band photospheric flux of 0.016 Jy (Acker et al. 1992) is significantly smaller than the observed value of 0.033 Jy.

The star seen about 2.″3 north of the central star is probably a field star seen in projection against the nebula. Even if it were located within the nebula, it is too far away from the central star to have affected its evolution.

## 4. Formation of the Etched Hourglass Nebula

### 4.1. The Large Hourglass Structure

What physical mechanism can produce the exquisite shape and structure of the Etched Hourglass nebula? In the Generalised Interacting Stellar Winds Model (GISW) for the formation of planetary nebulae (Kwok, Purton & Fitzgerald 1978, Balick 1987), axisymmetrical PNs shapes result when a fast (1000-2000 km $s^{-1}$ ), tenuous, post-AGB stellar wind expands within a slower (10-20 km $s^{-1}$ ), denser AGB CSE. The asymmetry may be intrinsic to the slow CSE (Balick 1987) or may be created by high-velocity ($\sim$100 km $s^{-1}$ ) collimated outflow(s) acting on an intrinsically round CSE (Sahai & Trauger (1998), hereafter ST98). Such high-velocity outflows are being discovered in an increasing number of young post-AGB objects (e.g. CRL2688: Young et al. 1992, Sahai et al. 1998a; HD101584: te Lintel Hekkert, Chapman & Zijlstra 1992). In MyCn18, the high-velocity knotty bipolar outflow (Bryce et al. 1997) favors the proposal by ST98.

Numerical models of the hydrodynamics of such interacting winds (Balick, Preston, & Icke 1987) produce a dense shell of swept-up gas with an hourglass shape when the equatorial-to-polar density contrast in the AGB CSE is relatively large ($\gtrsim$10). The open-ended hourglass geometry and the weak, filamentary emission seen in the [N II] and H$\alpha$ images outside the hourglass indicates that the fast outflow has broken out of the confining shell of swept-up gas along the polar directions into a surrounding more tenuous CSE (Garcia-Segura & Mac Low 1994). The thin shell of compressed gas which forms the walls of the hourglass is subject to various instabilities, including the Kelvin-Helmholtz, the Rayleigh-Taylor, and the "nonlinear thin shell" (Vishniac 1994) instabilities. These instabilities will act to produce locally overdense regions (Blondin & Lundqvist 1993, Dwarkadas & Balick 1998). Indeed, the arc-like etchings and mottlings appearing on the walls of the hourglass may be manifestations of such instabilities (Garcia-Segura et al. 1998). Borkowski, Blondin & Harrington 1997 have presented 2-D numerical hydrodynamical modelling of a poorly collimated outflow expanding into a confining ambient medium, in order to simulate the structure of the protoplanetary nebula He3-1475. The results of this simulation include the formation of a thin-walled shell which is smooth closer to the center of the nebula, but is broken up further away due to dynamical instabilities (see Fig. 3 of Borkowski, Blondin & Harrington 1997), qualitatively resembling the case of MyCn18, where the etchings and mottlings appear only in the more distant regions of the hourglass walls. Alternatively, the etchings may be the remnants of thin dense shells in the progenitor AGB CSE, similar to the arcs found in the protoplanetary nebula CRL2688 (Sahai et al. 1998b).

It is difficult to accurately constrain the properties of the progenitor dense AGB CSE which evolved into MyCn18 without the aid of detailed hydrodynamic modeling. However, we can make rough estimates of its mass-loss timescale and mass-loss rate. From our spatio-kinematic model in Paper 2, we find that (a) the mass of ionised gas in the hourglass walls is 0.013 $M_{\odot}$, (b) the expansion timescale for the walls is 1000–2000 yr, and (c) the density of the hourglass at a latitude of 32° (or $R = 1.3 \times 10^{17}$ cm) is about 1350 $\mathrm{cm}^{-3}$. We conservatively take the density of the undisturbed AGB CSE at this radius to be a factor 3 lower, to fit the large (∼factor 10) contrast in brightness between the H$\alpha$ intensity in the hourglass walls and neighbouring locations on the outside of the walls. Numerical GISW models of bipolar PNs with radiative losses show that this density contrast factor varies from ≈2–10 going from low to high latitudes (Mellema 1993). This would imply an AGB mass-loss rate, $\dot{M}_{AGB}$=2 $\times$ $10^{-6}$ $M_{\odot}\,\mathrm{yr}^{-1}$, assuming a typical AGB mass-ejection velocity, $V_{AGB}$=10 km $\mathrm{s}^{-1}$. Although we do not directly know what fraction of the AGB CSE has been swept up into the hourglass shell, it clearly must be a significant fraction, as the fast outflow has already broken out of the dense CSE. Assuming this fraction to be 1/2 and knowing the mass of the hourglass walls, we derive an AGB mass-loss time-scale of $\tau_{\mathrm{loss}} \approx 13000$ yr, a value roughly consistent with the 11000 yr required for the slow wind to reach the observed size of the nebula, and significantly larger than the expansion timescales for the hourglass walls.

### 4.2. The Central Region

The GISW model can qualitatively explain important features of the hourglass structure in MyCn18, but it does not address the complexities of the central region. These include the existence of the inner hourglass and Ring 2, and the offsets of the central star from the geometrical centers of the outer and inner hourglasses, Ring 1 and Ring 2.

The inner hourglass, like the outer hourglass, might also be produced by interacting winds. This would require the presence of a second, equatorially-concentrated, dense, slowly expanding CSE, interacting with a fast wind. Such a scenario has not been considered in the GISW model.

We have considered several mechanisms for producing the offset of the visible central star from the symmetry center of the outer hourglass. The simplest of these is that the nebula and the central star have an appreciable motion relative to the ambient ISM to the SW, the direction of the offset. The ram pressure of the ISM on the swept-up hourglass shell would reduce its proper motion relative to the star and give the observed offset. There are two problems with this mechanism. First, there is no obvious morphological signature on the SW side of the nebula indicating an external pressure – the nebula is remarkably symmetric. Second, the dynamical timescale of the waist of the outer hourglass (Ring 1) is $2\times10^{16}$ cm / 10 km $s^{-1}$ $\approx$700 yr[12]. This time scale is small compared to the 3500 yr sound-crossing time across the $\sim 10^{17}$ cm path through the progenitor AGB CSE which presumably surrounds the ionization-bounded waist of the nebula. The sound-crossing time is limited by the sound speed which is no greater than 10 km $s^{-1}$ in ionised gas and significantly smaller in the lower temperature neutral gas.

---

[12]since [O III] is much more centrally confined than [N II], the [O III] expansion velocity more accurately represents the expansion of the waist region

We now discuss mechanisms for producing the central star offset through an asymmetric mass-ejection of the progenitor AGB CSE. The first mechanism invokes a proper motion given to the star as a reaction to an intrinsic asymmetry in the mass-ejection of the progenitor AGB star. Over the course of a rotation period, the net reaction force on the star will of course be zero. Thus, the reaction must have acted for a time that is less than the rotational period of the progenitor AGB star (probably less than a few hundred years, scaling from the Sun's rotation period), and the star must have travelled to its current position in this time. This requires a proper motion of order 10 km $s^{-1}$ and a force of order $0.05 M_{\odot}$ km $s^{-1}$ $yr^{-1}$. This is significantly larger than the reaction that can be extracted from the wind ($<\dot{M}_{AGB} \times V_{AGB}$), which is of order $10^{-4} M_{\odot}$ km $s^{-1}$ $yr^{-1}$.

A second mechanism is one in which the central star is a close binary, with the more evolved star being the visible central star in our images. Mass transfer onto the surface of this star might have resulted in an explosive event which produced an expanding shell of ejecta and formed Ring 1. The center of mass of this shell would share the same velocity as the star in it orbital motion at the time of ejection, and since it would not be gravitationally bound to the binary system, it would move away from the binary system. We reject this model for the following reasons. The explosive event, qualitatively similar to a nova outburst due to thermonuclear runaway, is expected to eject a shell with velocities on the order of hundreds of $\mathrm{km\,s^{-1}}$ (Kovetz & Prialnik 1994, Shankar, Livio & Truran 1991). However, the long-slit spectrum of CS93 shows that the velocities in the inner regions of the nebula (Ring 1) are of the order of 10 $\mathrm{km\,s^{-1}}$. Secondly, the likely candidate for the star which donates material to the hot star is a red giant, but the observed $2\mu$m flux density of 0.033 Jy (see §3.3) is much lower than that expected for a red giant. For example, a $L = 3000\ L_{\odot}$ red giant with $T_{\rm eff} = 3000$ K produces a flux density of roughly 5.5 Jy at 2.4 kpc. Finally, this model also does not explain the offset of the central star with respect to the large hourglass structure.

The third mechanism invokes binarity of the central star (the companion to which is not seen and so must be less luminous). This admits the two cases of a close binary with a separation less than about 100 AU and a wide binary with a larger separation. Soker et al. (1998) have presented an analytical, highly idealized model of a close binary. The basic idea is that the net outflow speed of the ejected mass, averaged over many orbital cycles, might be different in different directions, and this will lead to an offset in the star's position from the center of symmetry of the resulting AGB CSE. This model may account for the offset of the central star from the center of Ring 1, but does not explain the offset of the star from the center of the extended hourglass structure. Nonetheless we believe it provides a plausible mechanism for producing an offset between the location of the central star and the center of symmetry of its ejecta, and deserves to be explored in greater detail.

For wide binaries, the orbital period may be comparable to or larger than the ejection timescale of the slow wind. Soker (1994) concludes that this will result in not only a displacement of the star, but may also produce large deviations from axisymmetry in the AGB CSE. Since MyCn18 appears to have a well-defined axis of symmetry, a wide binary scenario appears unlikely.

Our F547M image enables us to constrain the luminosity of any well-separated companion to the central star. Although this constraint is not useful for the close binary model (Soker et al. (1998)), it may be of value for new theoretical models. We find that the $3\sigma$ lower limit on $m_V$ for companions with separation of 500–1000 AU are 20.3–23.8 mag. The corresponding luminosity upper limits are roughly 0.1–0.004 $L_{\odot}$ if the companion is a cool star with $T_{eff} \sim 3500$ K, and roughly 25–1 $L_{\odot}$ if it is a hot white dwarf with $T_{eff} \sim 10^5$ K.

A binary star scenario is attractive for other reasons. Binarity can produce, directly or indirectly, asymmetries through the formation of a dense equatorial accretion/excretion disk (Morris 1987), high-velocity collimated outflows (Soker & Livio 1994, ST98), or an equatorially flattened common envelope (Livio 1993). In these contexts, Ring 1 may find a natural explanation as the dense equatorial waist of an hourglass-shaped PN produced via the GISW scenario. However, the origins of Ring 2 and the inner hourglass still remain a puzzle. It is noteworthy that inner and outer hourglass structures have been shown to exist in two other evolved objects whose central stars are symbiotic binaries – through direct imaging in the case of He2-104 (CS93, ST98), and through analysis of long-slit spectroscopic observations in R Aqr (Solf & Ulrich 1985). R Aqr also shows a jet-like outflow whose axis has changed over time (Hollis, Pedelty, & Kafatos 1997), supporting ST98's hypothesis that such outflows play an important role in the shaping of PN in general, and MyCn18, in particular (§4.1).

## 5. Conclusions

We have obtained emission-line and continuum images of MyCn18 with WFPC2 on HST. These images show an hourglass-shaped structure. A series of arcs appear to be etched on the walls of the larger, outer hourglass near its rims, giving it its name. Faint, distant, low-excitation blobs are found near the long axis of the nebula. These are probably part of the high-velocity bipolar outflow which has been observed previously in MyCn18.

In the complex central region of the nebula we find a smaller, inner hourglass and two rings. Ring 1 is a bright elliptical ring defining the outer hourglass waist. Ring 2 is a smaller, higher-excitation ring. The inner and outer hourglasses, & Ring 1 and Ring 2 have different centers and none are centered on the central star.

Although the GISW model for planetary nebula formation can qualitatively explain the shape and kinematics of the outer hourglass, the complex inner nebular structure and the offsets of the central star from the center of the nebula components remain a mystery. We believe that it is likely that a successful explanation of these will involve a binary central star.

This work was supported by NASA grant NAS 7-1260 to the WFPC2 IDT. We are grateful to Will Henney, Mark Morris, and Michael Richer for useful suggestions.

## REFERENCES


Acker, A., Jasniewicz, G., Koeppen, J., & Stenholm, B. 1989, A&AS, 80, 201

Acker, A., Ochsenbein, F., Stenholm, B., Tylenda, R., Marcout, J. & Schohn, S. 1992, Strasbourg-ESO Catalog of Galactic Planetary Nebulae, European Southern Observatory, Garching

Balick, B. 1987, AJ, 94, 671

Balick, B., Preston, H.L., & Icke, V. 1987, AJ, 94, 1641

Blondin, J. & Lundqvist, P. 1993, ApJ, 405, 337

Borkowski, K.J, Blondin, J.M. & Harrington, J.P. 1997, ApJ, 482, L97

Brown and Mathews 1970, ApJ, 160, 939

Bryce, M., Lopez, J.A., Holloway, A.J., & Meaburn, J. 1997, ApJ, 487, L161

Burrows, C., et al. 1995, ApJ, 452, 680

Corradi, R.L.M. & Schwarz, H.E. 1993, A&A, 268, 714

Dwarkadas, V.V. & Balick, B. 1998, ApJ, 497, 267

Garcia-Segura, G. & Mac Low, M. 1994, in Proc. 34th Herstmonceux Conf., ed. R.E.S. Clegg & I.R. Stevens (Cambridge University Press), 85

Garcia-Segura, G., Langer, N., Rozyczka, M. & Franco, J. 1998, ApJ, submitted

Gleizes, F., Acker, A. & Stenholm, B. 1989, A&A, 222, 2

Harrington, J.P., Lame, N.J., White, S.M., & Borkowski, K.J. 1997, AJ, 113, 2147

Herman, J., Burger, J.H., & Penninx, W.H. 1986, A&A, 167, 247

Hollis, J.M., Pedelty, J.A., & Kafatos, M. 1997, ApJ, 490, 302

Jura, M. 1986, ApJ, 303, 327

Kovetz and Prialnik 1994, ApJ, 424, 319

Kwok, S., Purton, C.R., & Fitzgerald, P.M. 1978, ApJ, 219, L125

Livio, M. 1993, in Planetary Nebulae, IAU Symposium 155, eds. R. Weinberger & A. Acker (Kluwer), p.279

Mayall, M.W. & Cannon, A.J. 1940, Harv. Bull. 913, 7

Mellema, G. 1993, in *"Numerical Models For the Formation of Aspherical Planetary Nebulae"*, Ph.D. thesis, Sterrewacht Lieden

Morris, M. 1987, PASP, 99, 1115

Osterbrock, D. E. 1989, in Astrophysics of Gaseous Nebulae and Active Galactic Nucleii, (University Science Books:Mill Valley)

Schwarz, H.E., Corradi, R.J.M. & Melnick, J. 1992, A&AS, 96, 23

Sahai, R., Wootten, A., Schwarz, H.E., Clegg, R.E.S. 1991, A&A, 251, 560

Sahai, R., Hines, D.C., Kastner, J.H., Weintraub, D.A., Trauger, J.T., Rieke, M.J., Thompson, R.I., & Schneider, G. 1998a, ApJ, 492, L163

Sahai, R., Trauger, J.T., Watson, A.M. et al. 1998, ApJ, 493, 301

Sahai, R. & Trauger, J.T. 1998, AJ, 116, 1357

Dayal, A. et al. 1999 (in preparation)

Shankar, A., Livio, M. & Truran, J.W. ApJ, 374, 623

Soker, N., Rappaport, S., & Harpaz, A. 1998, ApJ, 496, 842

Soker, N. 1994, MNRAS, 270, 774

Soker, N. & Livio, M. 1994, ApJ, 421, 219

Solf, J. & Ulrich, H. 1985, A&A, 148, 274

te Lintel Hekkert, P., Chapman, J.M., & Zijlstra, A.A. 1992, ApJ, 390, L23

Trauger, J.T. et al. 1994, ApJ, 435, L3

Tylenda, R., Acker, A., Stenholm, B., Gleizes, F., Raytchev, B. 1991, A&AS, 89, 77

Vishniac, E.T. 1994, ApJ, 428, 186

Young, K., Serabyn, G., Phillips, T.G., Knapp, G.R., Gusten, R., Schulz, A. 1992, ApJ, 385, 265

Zhang, C.Y., Harvey, P.M., Smith, B.J., Colome, C., DiFrancesco, J. 1994, ApJ, 425, 687

---

This manuscript was prepared with the AAS LaTeX macros v4.0.

Fig. 1.— Images of the young planetary nebula MyCn18, taken through narrow band filters with the Planetary Camera in WFPC2/HST to isolate atomic (or ionic) line emission: (a) F658N ([N II]$\lambda$6586) (b) F656N (H$\alpha$), (c) F502N ([O III]$\lambda$5007), and (d) a continuum filter, F547M. The plate scale is $0''.0456$/pixel, and the images cover an area $22''.8\times22''.8$ ($500\times500$ pixels). The linear streak in the upper right quadrant of the H$\alpha$ image is due to imperfect removal of a cosmic-ray event. A logarithmic stretch has been used in all images, and the maximum (black) and minimum (white) intensity values on the reverse grey-scales used (shown below each image) are (a) $8.43\times10^{-12}$ & $2.93\times10^{-15}$ erg s$^{-1}$ cm$^{-2}$ arcsec$^{-2}$, (b) $1.81\times10^{-11}$ & $3.67\times10^{-15}$ erg s$^{-1}$ cm$^{-2}$ arcsec$^{-2}$, (c) $1.47\times10^{-11}$ & $7.38\times10^{-15}$ erg s$^{-1}$ cm$^{-2}$ arcsec$^{-2}$, and (d) 6.53 & $5.95\times10^{-3}$ mJy arcsec$^{-2}$.

Fig. 2.— The inner $7''.75\times5''.92$ region of the nebula, seen in the emission lines of (a) [N II] (b) [O I]. (c) H$\alpha$, and (d) [O III]. A logarithmic stretch and reverse grey-scale have been used in all images, and the maximum (black) and minimum (white) intensity values on the reverse grey-scales used (shown below each image) are (a) $1.79\times10^{-11}$ & $3.56\times10^{-14}$ erg s$^{-1}$ cm$^{-2}$ arcsec$^{-2}$, (b) $3.53\times10^{-12}$ & $6.69\times10^{-15}$ erg s$^{-1}$ cm$^{-2}$ arcsec$^{-2}$, (c) $1.67\times10^{-11}$ & $4.19\times10^{-14}$ erg s$^{-1}$ cm$^{-2}$ arcsec$^{-2}$, and (d) $1.85\times10^{-11}$ & $2.33\times10^{-14}$ erg s$^{-1}$ cm$^{-2}$ arcsec$^{-2}$.

Fig. 3.— Radial cuts of the relative H$\alpha$, [NII] and continuum intensities taken along the long axis of the nebula, generated from the F656N, F658N and F547M filter images. The intensity traces for each filter have been scaled by arbitrary factors to avoid overlap. The thin (thick) curves refer to the NW (SE) lobe of the nebula.

Fig. 4.— (a) A composite color image of MyCn18 showing H$\alpha$ (green), [N II] (red), and [O III] (blue) emission (the color balance has been adjusted such that regions where the [N II] and H$\alpha$ overlap appear orange). The image covers an area $24''.59\times23''.32$ ($540\times512$ pixels). These images have been processed in order to emphasize sharp structures. The

processed image, $Im_P = Im_O/(Im_O + 0.04 Im_S)$, where $Im_O$ is the original image, and $Im_S$ is obtained by smoothing $Im_O$. The greenish linear streak in the upper right quadrant of the image is due to imperfect removal of a cosmic-ray event during the H$\alpha$ exposure. (b) the [N II]/H$\alpha$ ratio image, shown on a logarithmic scale. The maximum & minimum values of the ratio on the grey-scale used (shown alongside) are 0.134 & 1.48. Regions of the ratio image where the H$\alpha$ image has relatively low signal-to-noise have been masked and shown in green. (c) As in panel *b*, but for [O III]/H$\alpha$; maximum & minimum ratios on the grey-scale used are 0.055 & 1.76.

Fig. 5.— A composite color mosaic of [N II] (red), H$\alpha$ (green), and [O III] (blue) images from all 4 cameras in WFPC2. The intensities in the main nebula on the PC chip have been decreased by a factor 10 compared to the other 3 WF chips. The faint yellow nebulosities seen north of the main nebula represent low-excitation gas which was ejected from the central star at significantly higher speeds than the expansion velocity of the main nebula.

Table 1. Summary of HST/WFPC2 Observations

| Filter | Integration time | Line | Measured Flux |
|---|---|---|---|
| F656N | 600s | H$\alpha$ | $4.13\times10^{-11} erg\ s^{-1} cm^{-2}$ |
| F658N | 700s | [N II] | $3.43\times10^{-11} erg\ s^{-1} cm^{-2}$ |
| F631N | 700s | [O I] | $1.77\times10^{-11} erg\ s^{-1} cm^{-2}$ |
| F502N | 700s$\times$2 | [O III] | $7.44\times10^{-11} erg\ s^{-1} cm^{-2}$ |
| F547M | 200s | Continuum | 9.8 mJy |

[a] The $H\alpha$ image suffers from contamination by [N II], since F656N has about 4% transmission at [N II]$\lambda$6586, and 29% transmission at [N II]$\lambda$6548. The [N II] $\lambda$6548 line is 1/3 the strength of [N II]$\lambda$6586 in PNs on both observational (Acker et al. 1989) and theoretical grounds, hence the combined effect is equivalent to a 14% contamination by $\lambda$6586 (see e.g. Harrington et al. 1997). Since the [N II]$\lambda$6586 flux is $\approx$83% of the $H\alpha$ flux, the corrected $H\alpha$ flux should be $\approx$12% lower than the F656N flux value above; correspondingly, contamination of [N II]$\lambda$6586 by $H\alpha$ implies that the correct [N II]$\lambda$6586 flux is $\approx$5% less than the F658N flux value above.

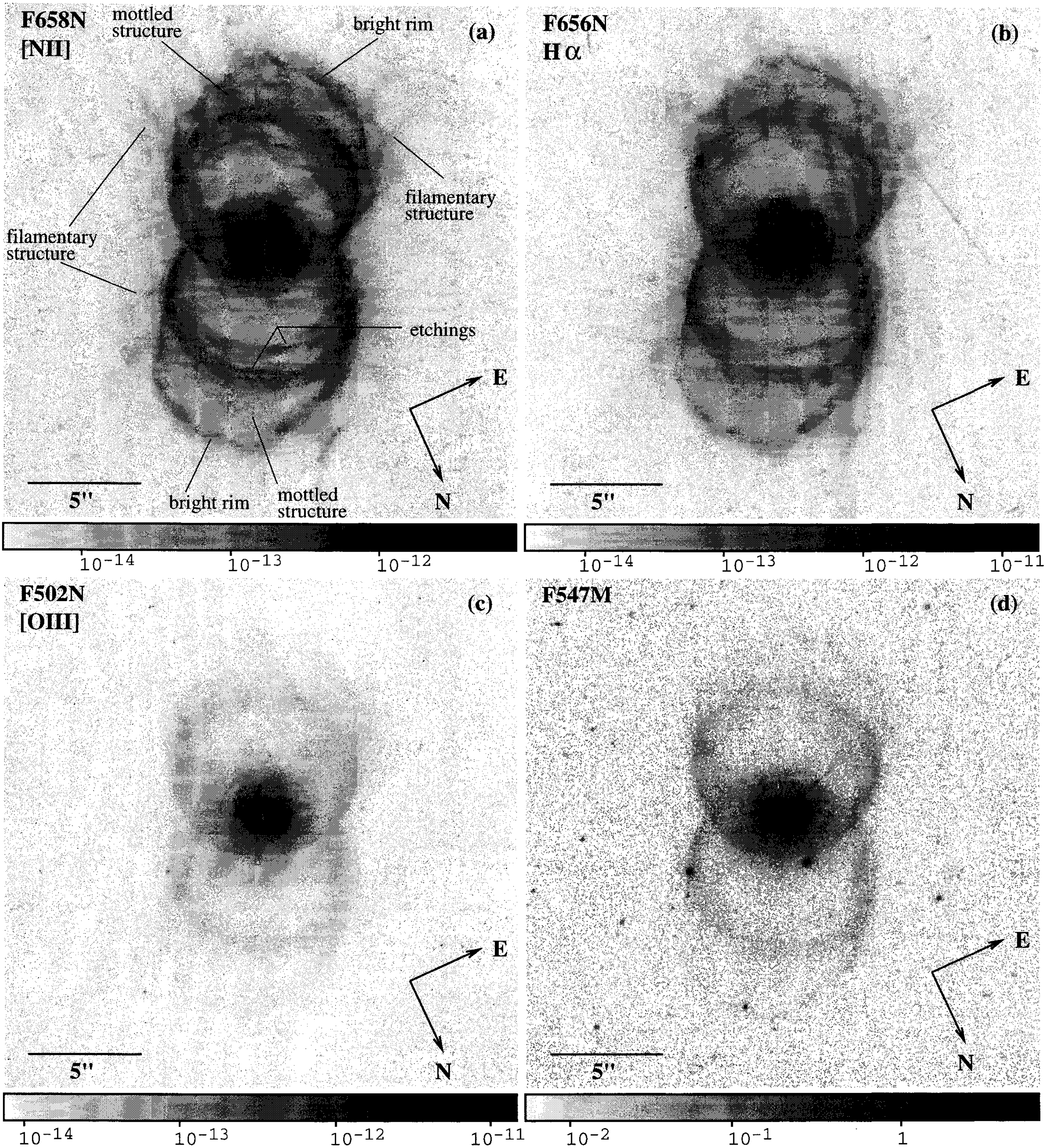

F658N
[NII]
mottled structure
bright rim
(a)
filamentary structure
filamentary structure
etchings
E
N
5''
bright rim
mottled structure
10−14
10−13
10−12
F656N
H α
(b)
E
N
5''
10−14
10−13
10−12
10−11
F502N
[OIII]
(c)
E
N
5''
10−14
10−13
10−12
10−11
F547M
(d)
E
N
5''
10−2
10−1
1

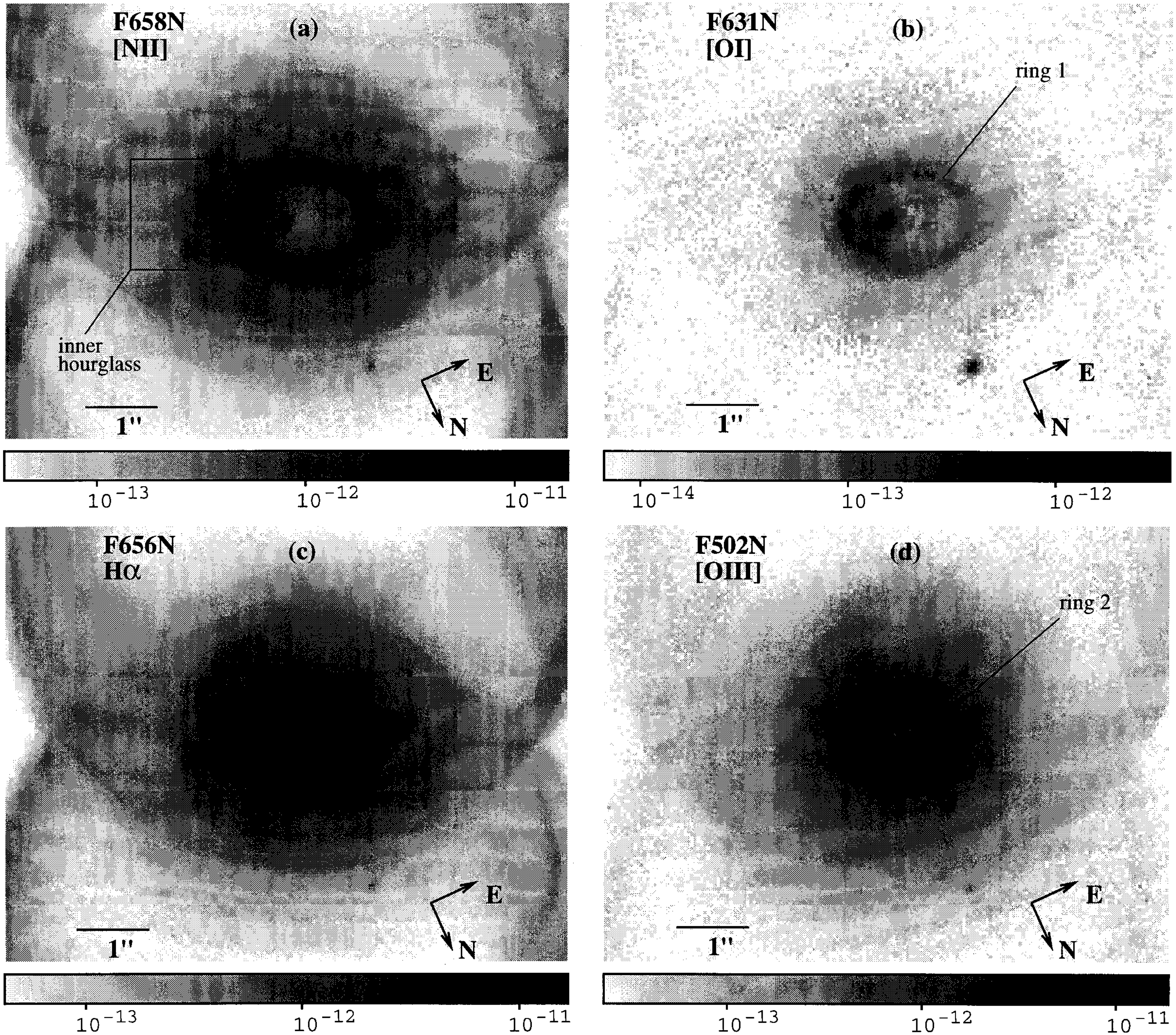
F658N
[NII]
(a)
inner
hourglass
E
N
1''
$10^{-13}$
$10^{-12}$
$10^{-11}$
F631N
[OI]
(b)
ring 1
E
N
1''
$10^{-14}$
$10^{-13}$
$10^{-12}$
F656N
Hα
(c)
E
N
1''
$10^{-13}$
$10^{-12}$
$10^{-11}$
F502N
[OIII]
(d)
ring 2
E
N
1''
$10^{-13}$
$10^{-12}$
$10^{-11}$

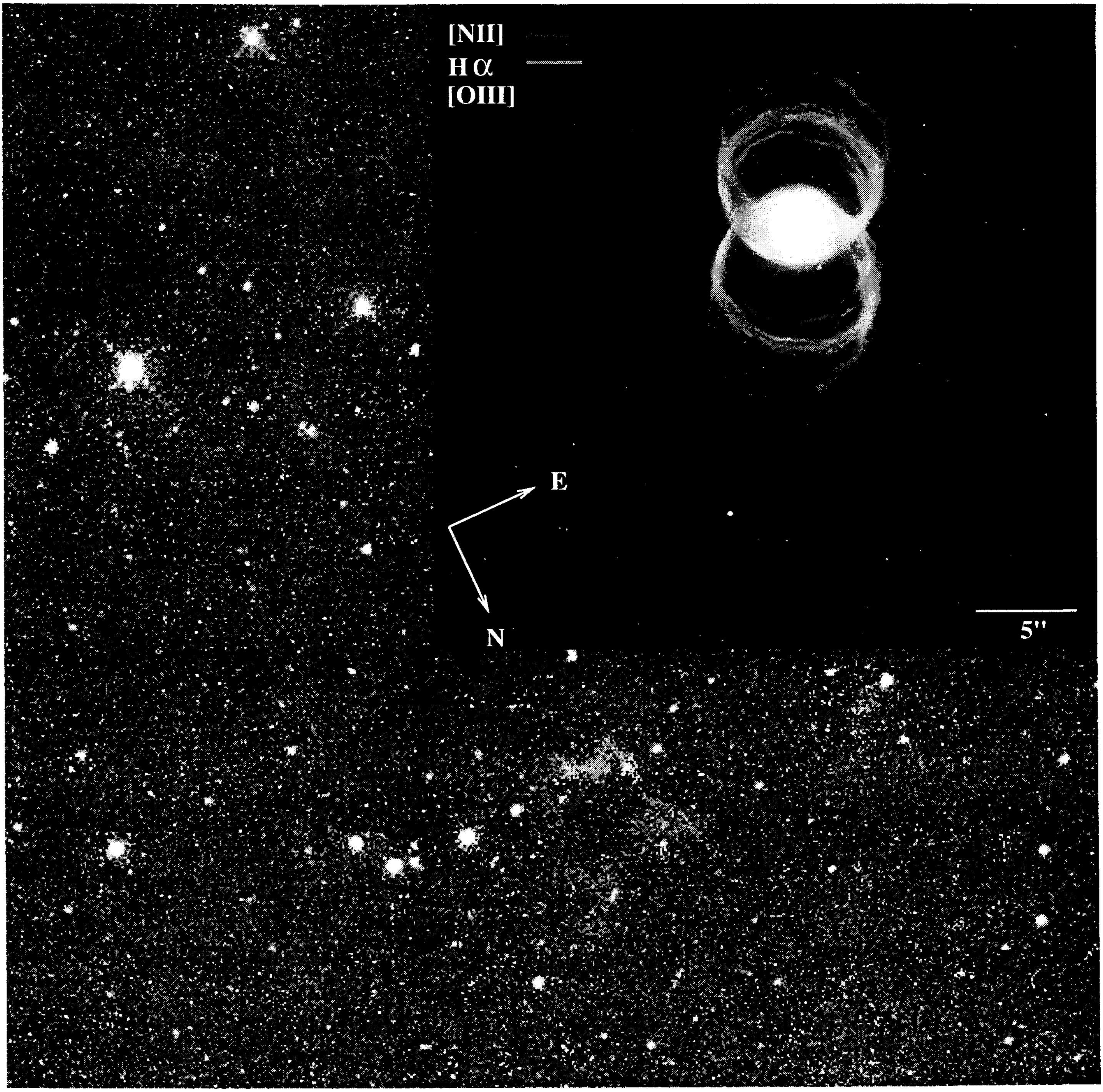
[NII]
H α
[OIII]
E
N
5"